Stem Cell Research & Therapy

RESEARCH

Open Access

Ameliorated cellular hallmarks of myotonic dystrophy in hybrid myotubes from patient and unaffected donor cells

Renée H.L. Raaijmakers[1,2,3], C. Rosanne M. Ausems[1,2,3], Marieke Willemse[3], Sarah A. Cumming[4], Baziel G.M. van Engelen[2], Darren G. Monckton[4], Hans van Bokhoven[1*†] and Derick G. Wansink[3*†]

Abstract

Background Cell-based strategies are being explored as a therapeutic option for muscular dystrophies, using a variety of cell types from different origin and with different characteristics. Primary pericytes are multifunctional cells found in the capillary bed that exhibit stem cell-like and myogenic regenerative properties. This unique combination allows them to be applied systemically, presenting a promising opportunity for body-wide muscle regeneration. We previously reported the successful isolation of *ALP*$^{+}$ pericytes from skeletal muscle of patients with myotonic dystrophy type 1 (DM1). These pericytes maintained normal growth parameters and myogenic characteristics in vitro despite the presence of nuclear $(CUG)_n$ RNA foci, the cellular hallmark of DM1. Here, we examined the behaviour of DM1 pericytes during myogenic differentiation.

Methods *DMPK* $(CTG)_n$ repeat lengths in patient pericytes were assessed using small pool PCR, to be able to relate variation in myogenic properties and disease hallmarks to repeat expansion. Pericytes from unaffected controls and DM1 patients were cultured under differentiating conditions in vitro. In addition, the pericytes were grown in co-cultures with myoblasts to examine their regenerative capacity by forming hybrid myotubes. Finally, the effect of pericyte fusion on DM1 disease hallmarks was investigated.

Results Small pool PCR analysis revealed the presence of somatic mosaicism in pericyte cell pools. Upon differentiation to myotubes, *DMPK* expression was upregulated, leading to an increase in nuclear foci sequestering MBNL1 protein. Remarkably, despite the manifestation of these disease biomarkers, patient-derived pericytes demonstrated myogenic potential in co-culture experiments comparable to unaffected pericytes and myoblasts. However, only the unaffected pericytes improved the disease hallmarks in hybrid myotubes. From 20% onwards, the fraction of unaffected nuclei in myotubes positively correlated with a reduction of the number of RNA foci and an increase in the amount of free MBNL1.

†Hans van Bokhoven and Derick G. Wansink contributed equally to this work.

*Correspondence:
Hans van Bokhoven
hans.vanbokhoven@radboudumc.nl
Derick G. Wansink
rick.wansink@radboudumc.nl

Full list of author information is available at the end of the article

Conclusions Fusion of only a limited number of unaffected myogenic precursors to DM1 myotubes already ameliorates cellular disease hallmarks, offering promise for the development of cell transplantation strategies to lower disease burden.

Introduction

Skeletal muscle abnormalities are a prominent feature in myotonic dystrophy type 1 (DM1). Patients often present with muscle wasting, muscle weakness and myotonia. The age of onset of these symptoms is highly variable and can present at birth to late adulthood, depending on the length of the expanded $(CTG)_n$ repeat in the 3′ untranslated region of the *dystrophia myotonica* protein kinase (*DMPK*) gene. The presence of >50 CTGs in blood is typical for the adult, classic form of DM1, whereas the inheritance of >1000 triplets usually leads to the severe, congenital form of the disease [1].

Current diagnosis of DM1 is performed by triplet repeat primed PCR (TP-PCR) on DNA from blood leukocytes. It is known that the $(CTG)_n$ repeat displays pronounced heterogeneity in somatic tissues. Consequently, the repeat length detected in peripheral blood leukocytes is generally not representative of the $(CTG)_n$ expansion in skeletal muscle, in which the repeat is usually much longer [2, 3]. Besides the length of the repeat, sequence alterations in the $(CTG)_n$ expansion may influence the severity of the phenotype. Most DM1 patients inherit a pure $(CTG)_n$ repeat expansion, but in a significant subset of individuals the repeat contains interruptions, reducing germline and somatic expansion, often associated with less severe symptoms and delayed disease onset [4].

The major pathogenic mechanisms suggested to contribute to the muscle phenotype of DM1 is linked to *DMPK* transcripts carrying an expanded repeat [5]. RNAs with $(CUG)_n$ expansions sequester splicing factors such as the muscleblind (MBNL) family of proteins, which can be visualized as RNA foci in cell nuclei. Additionally, the toxic effects exerted by these repeat-containing mRNAs include protein kinase C (PKC)-mediated CELF1 stabilization through hyperphosphorylation. In turn, the deregulated MBNL and CELF1 protein levels in DM1 cause a shift from an adult to a fetal splicing pattern of dozens of alternative splicing targets, including *MBNL1*, *MBNL2* and *DMD* [6, 7]. Misspliced transcripts ultimately lead to a perturbed protein imbalance in muscle and other affected tissues in patients with DM1.

While a variety of symptomatic and targeted treatments are currently being pursued [8, 9], no truly effective therapies for DM1 have yet been approved. In the development of a regenerative cell therapy for the skeletal muscle aspects of the disease, an important consideration is the selection of the cell type, which largely determines the proliferative capacity, the myogenic differentiation ability, and the route of administration [10–12]. Pericytes hold great potential as they can be isolated from skeletal muscle, have a proliferative capacity, and can differentiate into mature cells of different specificities, among which are myogenic precursor cells [10, 13–15]. The ease of isolation and the potential for systemic delivery favours pericytes over other myogenic cell types, such as satellite cells and myoblasts [16]. Over the last two decades, pericytes, or their embryogenic ortholog, mesoangioblasts, have been used in preclinical and clinical trials for Duchenne muscular dystrophy (DMD) [17–19], limb-girdle muscular dystrophy (LGMD) [20, 21] and mitochondrial myopathies (Clinical Trial ID: NCT05063721) [22], underscoring the possible value of the cell type for cellular therapies. We have previously shown that pericytes can be isolated from skeletal muscle of DM1 patients carrying different $(CTG)_n$ repeat lengths [12]. The intrinsic myogenic potential in vitro of these patient-derived pericytes appeared to be largely unaffected, despite the presence of typical disease hallmarks such as nuclear RNA foci formed by expanded *DMPK* transcripts [12].

In this study, we hypothesized that the DM1 cellular disease hallmarks differ between pericytes in the proliferation and their differentiated state, as myotube formation coincides with an induction of *DMPK* expression [23], leading to more *DMPK* mRNA production in myotubes. We therefore differentiated pericytes to myotubes and assessed the cultures for molecular hallmarks of DM1. We also wanted to assess the regenerative potential of pericytes in a cell therapeutic setting, therefore we fused pericytes of patients or unaffected individuals with DM1 myoblast-derived myotubes [24]. We then examined the co-cultures, to determine whether the unaffected pericytes could positively impact the DM1 disease characteristics of the myotubes.

Methods

Cell cultures

Human pericytes from six patients (P1-P6) and two unaffected controls (C1 and C2) were isolated, characterized and cultured as described in Ausems et al. [12]. Characteristics of the donors are summarized in Table 1.

DM2600 myoblasts (also called DM1 myoblasts) are immortalized cells that carry a $(CTG)_{13}$ and a $(CTG)_{2600}$ allele [25, 26]. The immortalized human myoblast line KM155C25 (C25 in short) was derived from an unaffected individual, carrying one $(CTG)_5$ and one $(CTG)_{14}$ allele [25, 26]. An isogenic line in which the DM1 $(CTG)_n$ repeat has been removed, DMΔ, was previously

Table 1 Primary pericyte cultures used in this study and patient characteristics

Donor	Sex	Disease/Control	MIRS	Age at biopsy (years)	Age of onset symptoms (years)	MRC degrees	Repeat length at diagnosis in blood (TP-PCR)	ePAL in blood washings (SP-PCR)	Modal repeat length pericytes (SP-PCR)
P1	M	DM1	5	46	18	5	$120 < N < 1000$	~110	360
P2	F	DM1	4	50	10	5	> 200	~150	950, > 1500
P3	F	DM1	4	39	12	4	> 200	~300	> 1500
P4	M	DM1	3	71	59	4+	50–150	~90	90, 115
P5	F	DM1	3	51	20	4+	> 150	n.i.	> 1500
P6	F	DM1	2	29	16	5	52	n.i.	60
C1	M	Control	n.a.	45	n.a.	n.a.	n.a.	n.a.	n.a.
C2	F	Control	n.a.	22	n.a.	n.a.	n.a.	n.a.	n.a.

generated from immortalized DM2600 myoblasts [25]. Cells were cultured as described [25].

The ViraPower Lentiviral Expression System (Life technologies) was used to facilitate lentiviral-based expression of H2B-GFP in immortalized DM1 myoblasts and H2B-mCherry in DMΔ myoblasts [27, 28]. Lentiviral particles containing pLenti6.2v5-H2B-eGFP (Invitrogen) and pLenti6.2v5-H2B-mCherry (a gift from A. J. C. de Groof, Nijmegen, The Netherlands), were used, followed by antibiotic blasticidin selection (10 mg/mL; Thermo Fisher Scientific, R2101) and fluorescence-activated cell sorting (FACS Aria SORP, Becton Dickinson) to generate stable cell lines.

$(CTG)_n$ repeat length was determined in blood at diagnosis (triplet repeat primed-PCR (TP-PCR)) and in isolated pericytes (small pool-PCR (SP-PCR)). M: male; F: Female; DM1: DM1 patient; MIRS: muscular impairment rating scale; n.a.: not applicable; n.i.: not included. Muscle strength in MRC degrees: strength measure of quadriceps. n.a.: not applicable. ePAL: estimated progenitor allele length by SP-PCR from blood washings. Multiple sizes found in column modal repeat length (in pericytes by SP-PCR) imply multiple clonally expanded pericytes with mode as mentioned.

Small pool PCR (SP-PCR)

SP-PCR was used for $(CTG)_n$ repeat length determination in the primary pericytes and blood washings [12]. DNA from purified pericytes and blood washings was isolated using the QIAamp DNA Mini Kit (QIAGEN™) according to the manufacturer's protocol. DNA concentrations were precisely measured with Qubit™ dsDNA HS Assay Kit (Thermo Fisher Scientific, Invitrogen™). DNA was diluted to 500 pg/uL template DNA per reaction. Repeat length was determined using SP-PCR amplification of the $(CTG)_n$ repeats and Southern blot hybridisation as described [29]. Flanking primers were DM-C (5'-AACGGGGCTCGAAGGGTCCT-3') and DM-DR (5'-CAGGCCTGCAGTTTGCCCATC-3'), which bind 34 bp upstream and 72 bp downstream of the repeat, respectively. Thus, the PCR amplification obtained with these primers adds 106 bp flanking sequence to the repeat length. To facilitate the amplification of the GC-rich repeat expansion, we added 10% dimethyl sulfoxide (DMSO) to the reaction. For visualization, 30 ng of a double-stranded DNA probe containing 56 CTG/CAG triplets was labelled with [α^{32}P]dCTP (3,000 Ci/nmol) from Perkin Elmer (NEG513H, Easytides). This solution mix was made according to the recommendations of the random primers DNA labelling system (Thermo Fisher 18187013). Six ng of the DNA size ladder was included with the labelling, so that the molecular-weight size markers (1 kb Plus DNA Ladder, Thermo Fisher Scientific, Invitrogen™) could also be visualized on the final autoradiograph. At least three reactions per template were performed. A negative no-DNA control and positive control were always included.

The inherited repeat length (the estimated progenitor allele length; ePAL) was determined by the lower boundary of the expanded alleles in blood washings DNA [30], ePAL was not determined for P5 as these samples were not able to be judged from the SP-PCR results (Suppl. Fig. 1), nor for P6, as washings were not taken during pericyte isolation. Modal allele length(s) were determined by the densest point(s) of the distribution of alleles. These measures were estimated using CLIQS 1D gel analysis software (TotalLab UK Ltd., Version 1.1) by comparison against the molecular weight marker.

All samples were screened for variant repeats according to the protocol of Cumming et al. [31] (data not shown). DMSO (10%) was included in the amplification reaction (Merck molecular biology grade) and the annealing temperature was lowered to 63.5 °C to improve denaturing/annealing of highly CG-rich templates. Half of the reaction mix after amplification was digested with the restriction enzyme AciI (New England Biolabs UK Ltd). The digested and non-digested samples were resolved side by side on the gel.

Fluorescent labelling of MBNL1 antibodies

MB1a antibody (Developmental Studies Hybridoma Bank (DSHB), University of Iowa) was produced by hybridoma

cell line 4A8 after serum starvation [32]. From the culture supernatant, the antibodies were isolated using Protein G Sepharose 4 Fast Flow antibody purification resin (GE Healthcare). Buffer exchange to phosphate buffered saline (PBS) and purification were subsequently performed using Amicon® Ultra-4 10 KDa cut-off centrifugal filters (Merck-Millipore). Antibodies were labelled by mixing a 1:5 molar ratio of antibody to Alexa Fluor© 647 NHS Ester (Thermo Scientific) and incubating at room temperature for 1 h. Free label was removed using 40 kDa cut-off Zeba™ Spin Desalting Columns (Thermo Scientific). The protein concentration was determined with a NanoVue Plus spectrophotometer (GE Healthcare), as was the degree of labelling. On average 3.1 fluorophore groups per antibody molecule were measured.

$(CUG)_n$ RNA FISH and immunofluorescent MBNL1 staining

For $(CUG)_n$ RNA foci and MBNL quantification, 10,000 cells were plated in proliferation medium in Ibidi 8-well chambers. At confluency, the medium was changed to differentiation medium. After six days in differentiation medium, myotubes were fixed in 2% paraformaldehyde (PFA) in 0.1 M phosphate buffer (pH 7.4) for staining. After washing 3 times with 1x PBS, permeabilization took place with 0.1% Triton X-100, 0.1% glycine and 3% bovine serum albumin (BSA) in PBS for 5 min. Following permeabilization, blocking for 1 h at room temperature in blocking buffer (0,1% glycine, 3% BSA) took place and cells were incubated overnight with directly labelled anti-MBNL1 antibody in blocking buffer (1:10) and anti-MHC antibody (1:50; MF20 DSHB, University of Iowa). After washing 3 times with 1x PBS, cells were incubated with 2 µg/mL goat anti-mouse Alexa Fluor 488 and 100 ng/mL 4′,6-diamidino-2-phenylindole (DAPI; Sigma-Aldrich) in blocking buffer for 1 h at room temperature in the dark. Cells were washed 3 times with and imaged in 1x PBS.

For RNA FISH, we followed the Stellaris FISH protocol (Biosearch Technologies) for overnight labelling. Both FISH probes (12.5 µM) consisted of DNA and locked nucleic acid (LNA) nucleotides and were diluted 100x. The $(CAG)_6$ probe was labelled with TYE563 (Exiqon, Vedbæk, Denmark): 5'-TYE563-CAGCAGCAGCAGCAGCAGC-3'. After washing 3 times with 1x PBS, blocking took place for 5 min and cells were incubated overnight in anti-MHC antibody (1:50). After washing 3 times with 1x PBS, cells were incubated with goat anti-mouse Alexa Fluor 488 and 100 ng/mL DAPI in blocking buffer for 1 h at room temperature in the dark. Cells were washed with and imaged in 1x PBS.

Fluorescent images were acquired using a Zeiss LSM880 microscope. Images were analysed using Fiji imaging software. A mask based on MHC immunofluorescent staining was set visually. DAPI-positive nuclei were recognized via the auto-threshold "IsoData white" applying the "Fill Holes" option and a watershed on the binary image to separate overlaying nuclei and automatic cell count using "analyze particles" (settings: 10,000 to infinity for pixel size). Total nuclei and nuclei inside the MHC mask were quantified to determine myogenic fusion index (MFI). Within the nuclear selection, the "spot counter" function was used to quantify foci using a noise tolerance of 50.

RT-qPCR

Pericytes were differentiated for six days and RNA was isolated from cell pellets of proliferating and differentiating pericyte cultures using the NucleoSpin RNA isolation kit (Macherey-Nagel) according to the manufacturer's protocol. The RNA yield and purity per sample were determined by absorbance at 260/280 nm. RNA (2 µg) was reversed transcribed and cDNA was made by using random hexamers from the iScript cDNA synthesis kit according to the manufacturer's protocol (Bio-Rad Laboratories). A 40-fold diluted cDNA sample (5 µL) was mixed in a final volume of 25 µL containing GoTaq qPCR Master Mix, distilled H_2O, and 0.4 pmole of each primer. Samples were analysed using the QuantStudio™ 3 Real-Time PCR System (Thermo Fisher). No-template (NTC) and no-reverse-transcriptase (NRT) were included as negative controls. Gene-of-interest levels were normalized to the three reference genes *HPRT1*, *TBP* and *GAPDH* using qPCR software (QuantStudio Design & Analysis Software, Version 1.4.3). PCR primers used were as follows: *DMPK* e15-3′, 5′-TGCCTGCTTACTCGGGAAA-3′ and 5′-GAGCAGCGCAAGTGAGGAG-3′; *MHCp* (MYH8) e16-17 5'-ACATTACTGGCTGGCTGGACA-3' and 5'-CACCTTTCTTCGCGCTGCT-3'; *HPRT1* e7–e9, 5′-TGACAGTGGCAAAACAATG-3′ and 5′-GGTCCTTTTCACCAGCAAGCT-3′ and *GAPDH* 5'-CCCGCTTCGCTCTCTGCTCC-3' and 5'-CCTTCCCCATGGTTCTGAGCG-3'; *TBP* e3, 5′-CCACTCACAGACTCTCACAAC-3′ and 5′-CTGCGGTACAATCCCAGAACT-3′.

Co-culture of myoblasts and pericytes

For the fusion capacity experiment, DM1 myoblasts stably expressing H2B-GFP were grown to confluency in Ibidi µ-slide 8-well (Ibidi GmbH, Germany) plates. The proliferation medium was replaced by differentiation medium [25]. On day two of differentiation, 40,000 proliferating pericytes per well were added. After five days of co-culture, on day seven of differentiation, co-cultures were fixed and incubated with anti-MHC antibody as described above. Cells were incubated with 2 ug/mL goat anti-mouse Alexa Fluor 568 and 100 ng/mL DAPI (Sigma-Aldrich) for 1 h in the dark to stain all nuclei. Cells were washed three times with and imaged in 1x PBS. For quantification, a tile scan of the well was

acquired using a Axio Observer.Z1/7 with Sample finder microscope (Plan-Apochromat 20x/0.8 M27 with DAPI excitation filter: 375–395, emission filter 410–440; GFP: excitation filter 455–483, emission filter 499–529 and mCherry: excitation filter 545–565, emission 579–604, 3×3 binning). Wells were split in four quarters and were analysed for the myogenic fusion index (i.e., the number of nuclei in MHC^+ myotubes expressed as a percentage of the total number of nuclei in the culture). Similarly, the percentage of pericyte nuclei (H2B-GFP^-) in MHC^+ structures was determined using Fiji imaging software using the StarDist plugin in a macro (Suppl. Data 1 and 2) [33].

To study the effect of pericytes on disease characteristics in DM1 nuclei in co-cultures with differing percentages of pericyte nuclei per myotube, we either grew DM1 H2B-GFP myoblasts or pericytes to full confluency in µ-slide 8-well (Ibidi GmbH, Germany) plates. Again, on day two of differentiation, 40,000 proliferating cells (either pericytes or DM1 H2B-GFP myoblasts, respectively) were added. Similar culturing procedures, as well as fixation were performed for these cultures. However, we followed staining procedures as mentioned in the aforementioned paragraph: $(CUG)_n$ RNA FISH and MBNL1 staining. Myotubes were determined by overlapping brightfield images. Fluorescent images were acquired using a Zeiss LSM880 microscope. Images were analysed using Fiji imaging software.

Co-cultures of DM1 H2B-GFP myoblasts and DMΔ H2B-mCherry myoblasts were grown on WillCo-dish (WillCo Wells, The Netherlands) to demonstrate protein spreading over time [34]. DMΔ H2B-mCherry DMΔ myoblasts were added to DM1 H2B-GFP cells at day two of differentiation as described above. The co-cultures were fixated after 5, 10, 14 and 20 days of differentiation and stained for MHC as described in our fusion capacity experiments. Images were acquired using a Leica DMI6000B microscope (20x magnification N/A 0.5 with filter set Quad sedat DAPI/ FITC/ TRITC/ Cy5).

Statistical analyses

Statistical analyses were performed using GraphPad PRISM 9.0.0 (GraphPad Software, Inc., CA, USA). Data is shown as bar graphs with error bars expressing the mean±standard error of the mean (SEM), or in violin plots with solid lines representing the median and dotted lines representing the quartiles. In all figures, p-values are indicated as follows: <0.05 (*), <0.01 (**), <0.001 (***), <0.0001 (****). Normality was ensured using a Shapiro-Wilk test. For Fig. 6, a post-hoc Dunn's test for multiple comparisons was performed on dependent parameters when applicable.

Results

Characterization of $(CTG)_n$ repeat-length mosaicism in primary DM1 pericytes

Primary pericytes were isolated from quadriceps muscle biopsies from six DM1 patients and two unaffected controls, as described [12] (Table 1). The $(CTG)_n$ repeat length at the *DMPK* locus of patients was originally estimated in blood DNA by TP-PCR at the time of diagnosis. However, it is well-known that $(CTG)_n$ repeat lengths in DM1 are generally larger in skeletal muscle than in blood [2, 3]. We therefore performed small-pool PCR to determine (i) the progenitor allele length (ePAL), the repeat length the patient inherited from their parent in blood DNA, (ii) the modal allele length(s) in the pericyte cultures, and (iii) the degree of somatic mosaicism in the cells [35] (Fig. 1, Suppl. Fig. 1). Finally, we tested for the presence of variant repeats by post-PCR digestion with restriction endonuclease AciI, which cleaves CCG and CGG variant repeats [36].

In general, the pericyte repeat lengths all fell within the broad range given by TP-PCR from blood at diagnosis and none of our samples contained AciI-sensitive repeat variants (data not shown) [37]. For P1, P2, P4 and P6 distinct modal lengths were present. Specifically for P1, P2 and P4, multiple hybridization signals indicated extensive somatic $(CTG)_n$ repeat length mosaicism, ranging up to differences of several hundreds of triplets in P1 and P2. The rare large, but measurable expansions observed in P1, P2, P3, P4 and P5 may represent in vitro variants of cultured progenitors, or additional clonal progenitors that have not expanded as rapidly as the primary clones leading to multiple modal repeat lengths measured (e.g., P2 with modal lengths at 700 and 950 triplets) (Fig. 1; Table 1). The ePAL of P1 and P2 were established from blood washings of biopsies (Suppl. Fig. 1, Table 1) at approximately ~110 and ~150 triplets respectively, at ~300 for P3, while it was ~90 triplets for P4. No ePAL was determined for P5, as the repeat length exceeded the limitation, which might be due to insufficient material from blood washings, no blood washings were obtained for P6, hence an exact determination of mode and ePAL was not feasible for these two samples (Suppl. Fig. 1 and Table 1).

DM1 pericytes show an increased number of RNA foci upon myogenic differentiation

To examine pericyte behaviour during myogenic differentiation, we decided to concentrate on pericytes derived from C1, P2, P4 and P6. We previously established that pericytes from both patient and control pericyte populations maintain myogenic capacity in vitro and form multinucleated MHC^+ myotubes under differentiating conditions [12]. This is now confirmed by an increase in expression of *DMPK* and differentiation marker *MHC*

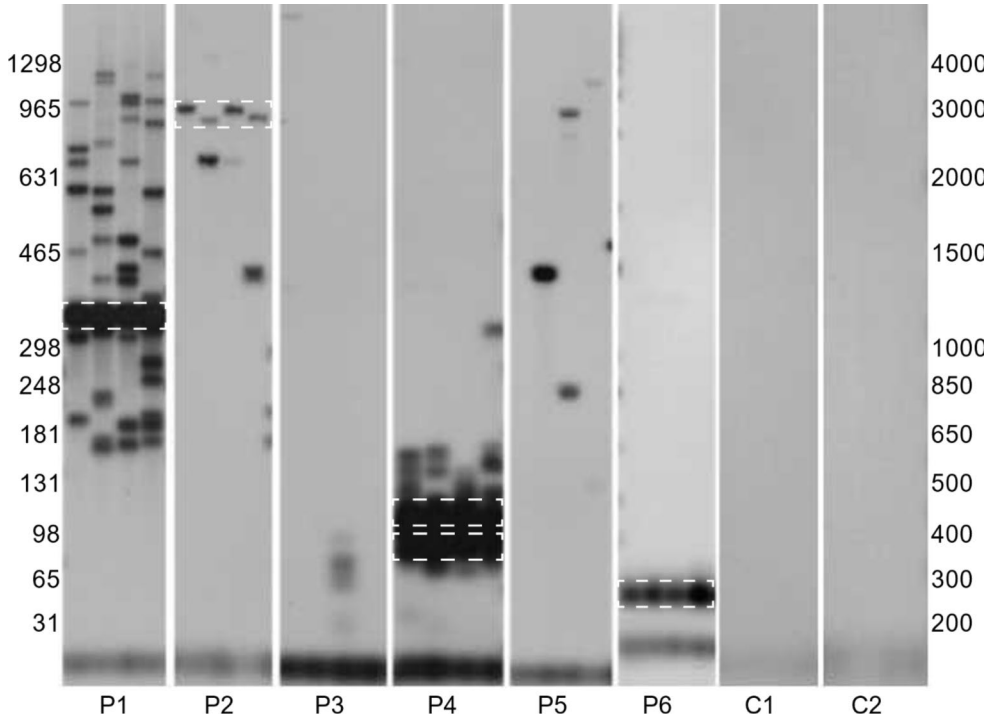

Fig. 1 Modal $(CTG)_n$ repeat-length determination in primary pericyte cultures from patients with DM1. SP-PCR was used for repeat length determination in pericytes. For each sample, four replicate PCRs were performed. The modal repeat length in patient pericytes is visible as the densest point of the distribution of alleles. The lengths of P3 and P5 could not be determined, and are therefore presumably > 1,500. Non-disease-causing alleles can be seen at the bottom of each gel. The marker on the left indicates the number of triplets, the right marker is in base pairs. For clarity, pericyte lanes of full-length blots were cropped and included in this figure. Full-length blots are presented in Supplementary Fig. 1

(Fig. 2A), albeit showing clear differences in the myogenic fusion capacity between the lines (P4 showing a relatively low increase in myogenic fusion efficiency, by the modest increase in *MHC* and *DMPK*). In MHC^+ cells of patients P2 and P4, increased *DMPK* expression coincides with an increase in $(CUG)_n$ RNA foci number (Fig. 2B, C). No foci were detected in differentiated cells from P6 despite a 20-fold increase in *DMPK*. This observation may reflect a true absence of nuclear retention of the mildly expanded *DMPK* RNAs, but more likely is caused by a detection limitation due to presence of only 60 CTG triplets.

Increased nuclear MBNL1 foci number parallels decreased free nuclear MBNL1 protein abundance

The current favoured hypothesis in the field is that nuclear $(CUG)_n$ RNA foci sequester proteins of the MBNL family, thereby depleting free MBNL protein from the nucleoplasmic pool [6, 7]. Thus, we wondered whether presence of expanded *DMPK* transcripts would also affect nuclear MBNL1 protein localization in differentiating pericyte populations. Immunofluorescence microscopy indeed showed that the nuclear distribution of MBNL1 was altered in six-day old MHC^+ pericyte-derived myotubes with an elongated $(CTG)_n$ repeat as compared to the MHC^- cells in the culture. Nuclear MBNL1-positive foci counts were similar to FISH-detectable $(CUG)_n$ RNA foci (Figs. 2B and 3A) [12]. A significant increase in MBNL1 foci number was detected for P2 ($p<0.001$) and P4 ($p<0.001$) in pericyte-derived myotubes. The normally bright, homogenous MBNL1 distribution in pericytes changed towards a pattern of MBNL1-enriched foci on a weaker nucleoplasmic background (Fig. 3B). Consistent with the RNA FISH data, no MBNL1 foci were detected in cells from patient P6 and control cells, showcasing a repeat-dependent effect on MBNL sequestration.

Careful quantification of MBNL1 staining in individual cells through advanced image analysis confirmed a reduced nucleoplasmic MBNL1 intensity in myotube nuclei from P2 ($p<0.001$) and P4 ($p<0.001$) (Fig. 3C) compared to non-differentiated cells in culture. The average P2 and P4 myotube nuclear MBNL1 protein staining was also lower than in nuclei in myotubes from unaffected (C1) and short-repeat containing (P6) for which MBNL1 intensity was similar in nuclei of MHC^+ and MHC^- cells. All in all, these observations suggest a sequestration model of MBNL1 protein concentration across the nucleus.

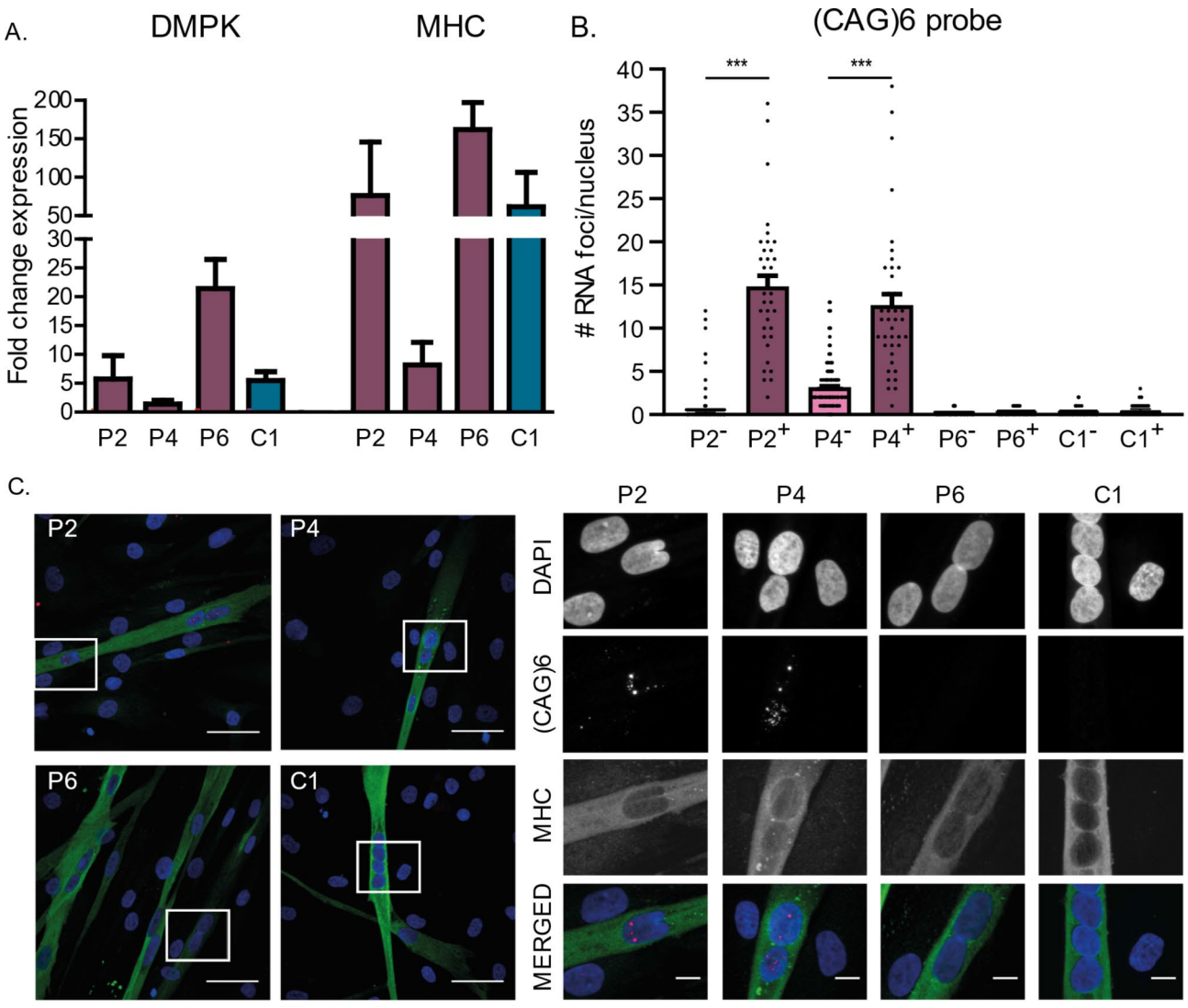

Fig. 2 $(CUG)_n$ RNA foci number in pericytes increases during myogenic differentiation **(A)** Fold change expression of *DMPK* and *MHC* during differentiation as determined via RT-qPCR (three independent differentiation experiments; mean ± SEM. Reference sample: undifferentiated pericytes, data not shown). **(B)** Quantification of $(CUG)_n$ RNA foci in nuclei of MHC-negative cells ("-") and MHC-positive myotubes ("+") using a $(CAG)_6$ probe. Each dot represents the foci number in one nucleus. For MHC-negative nuclei $n = 103$ to 218, for MHC-positive nuclei $n = 32$ to 40. Three independent differentiation experiments; mean ± SEM; *** $p < 0.001$, Mann Whitney U-test. **(C)** Representative FISH images of $(CUG)_n$ RNA foci in nuclei within MHC-negative cells and MHC-positive myotubes. MHC staining is shown in green, $(CUG)_n$ RNA foci in red, nuclei (DAPI) in blue. Scale bar in overview images = 50 µm. Scale bar in cut-outs = 10 µm

DM1 pericytes and unaffected pericytes contribute equally to hybrid myotube formation in vitro

To determine the therapeutic potential of pericytes as transplantable muscle progenitor cells, it is of utmost importance to investigate their regenerative potential. This concept is different from their intrinsic myogenic potential, where pericytes by themselves form MHC^+ multinucleated myotubes. To establish the regenerative potential of our unaffected and DM1 pericyte populations in vitro, pericytes were added to an existing differentiating culture of DM1 H2B-GFP-labeled myoblasts with a *DMPK* allele of 2,600 triplets at day two of differentiation (Fig. 4A) and fixed and stained for MHC at day 5 of differentiation (Fig. 4B).

Co-cultures were analysed for the presence of MHC^+ myotubes to determine the overall myogenic fusion index (MFI). The MFI was defined as the proportion of nuclei in MHC^+ cells expressed as a percentage of the total number of nuclei present in the culture. The hybrid cultures showed comparable MFIs of 17.2 to 38.4% (Fig. 4C).

Next, we wondered if the length of the expanded repeat in the patient-derived pericytes affected their contribution to the formation of hybrid myotubes. We established the presence of pericytes in hybrid myotubes by quantifying the number of pericyte nuclei (non-green) in MHC^+

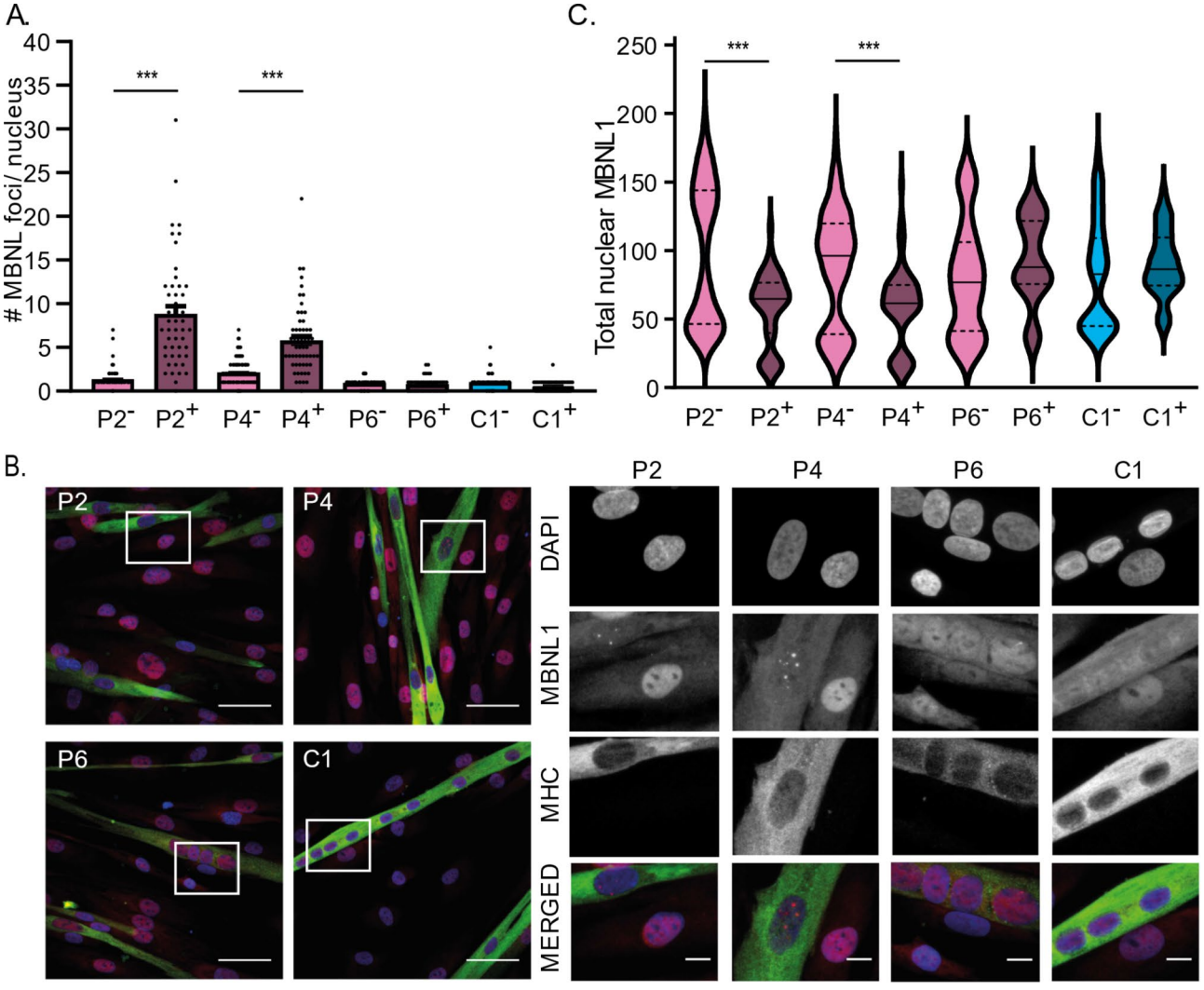

Fig. 3 MBNL1 localization in pericyte nuclei changes during differentiation. **(A)** Quantification of MBNL1 foci and **(C)** MBNL1 nucleoplasmic staining (total nuclear MBNL1 in grey values ranging from 0 to 255) in differentiating pericyte cultures. Each symbol represents one nucleus. For MHC-negative nuclei ("-") $n = 99$ to 153 for MHC-positive nuclei $n = 43$ to 58. MHC-positive myotubes ("+") with repeat lengths 90, 115 (P4) and 700, 950, < 1,500 (P2) showed a significant increase in MBNL1 foci number and a decreased nuclear intensity (three independent differentiation experiments; mean ± SEM; *** $p < 0.001$, Mann Whitney U-test). **(B)** Representative images of MBNL1 staining in nuclei in MHC-negative cells and in MHC-positive myotubes. Pericytes derived from three DM1 patients with variable repeat lengths were included. Myosin heavy chain (MHC) staining is shown in green, MBNL1 signal in red, DAPI in blue. Scale bar in overview images = 50 µm. Scale bar in cut-outs = 10 µm

myotubes formed by DM1 H2B-GFP-labeled myoblasts (green nuclei). All pericyte cultures from patients showed a similar contribution range to myotube formation in co-cultures (2.2 to 5.7%) compared to pericytes derived from unaffected controls (3.2 to 4.1%) (Fig. 4C). Furthermore, no differences were found between the addition of pericytes and myoblasts to the myotube formation, although unaffected myoblasts (C25) showed the highest total contribution at 8.7%. Also, after normalization to the total MFI of the co-cultures, no significant difference between the pericyte populations was observed in their capacity to contribute to myotube formation (Fig. 4D).

Fusion of unaffected pericytes ameliorates the severity of DM1 hallmarks in hybrid myotubes

To examine whether after fusion unaffected pericytes contributed a therapeutic effect at the cellular level, we decided to investigate DM1 disease hallmarks in hybrid myotubes. Co-cultures were started with either DM1 H2B-GFP myoblasts or with pericytes (C1, C2, or P4) followed by the addition of pericytes (C1, C2, or P4) or DM1 H2B-GFP myoblasts, respectively. After co-culturing for five days, heterogeneous populations of hybrid myotubes were formed, covering the full range in composition from 0 to 100% nuclei from unaffected donors (Fig. 5A). Co-cultures were fixed and stained for $(CUG)_{exp}$ RNA by

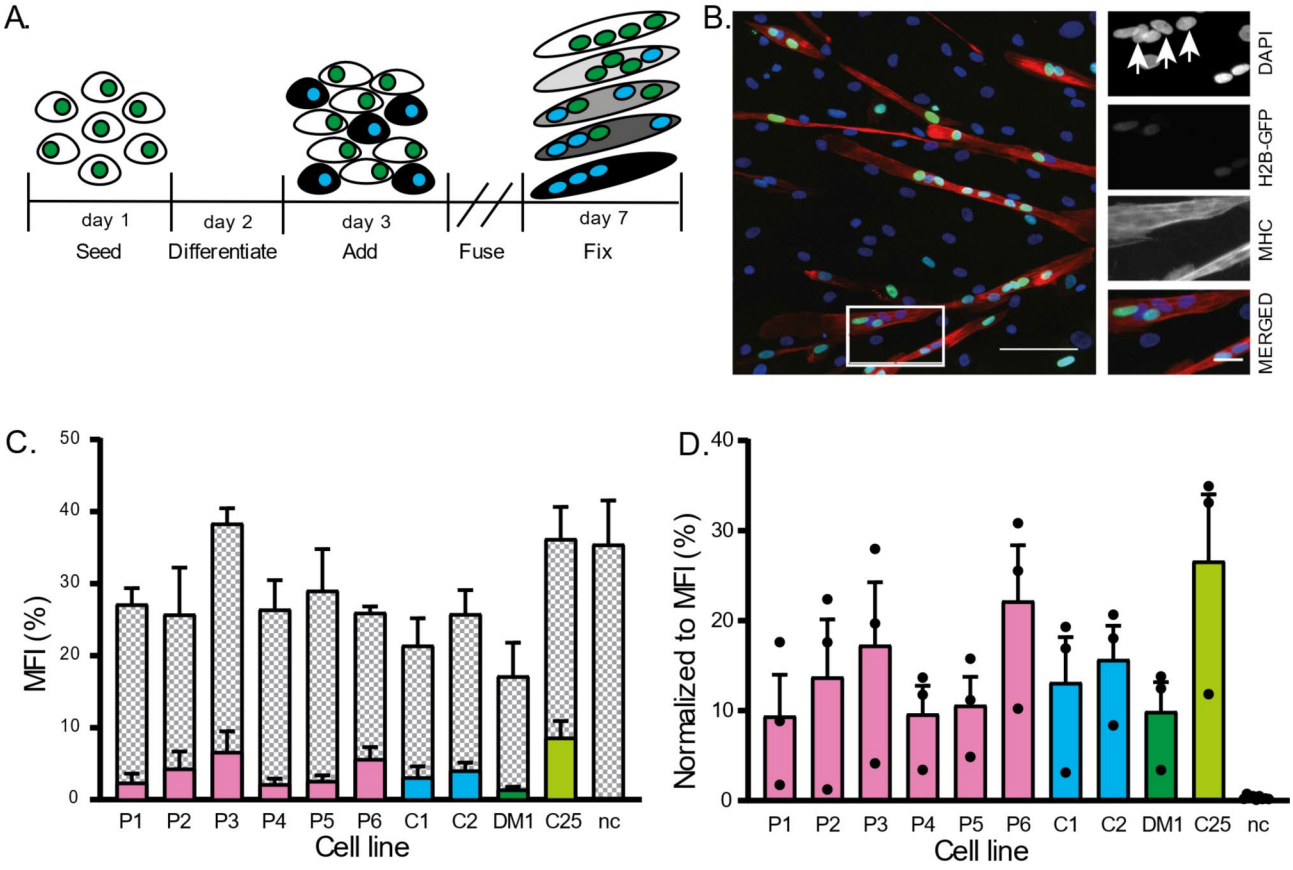

Fig. 4 Capacity of pericytes to fuse to differentiating DM1 myoblast-derived myotubes. **(A)** Graphical visualisation of the experiment. DM1 H2B-GFP cells (green) were seeded at day 1, the next day medium was replaced by differentiation medium and on day 3 pericytes were added. At day 7 myotubes were fixed for analysis. **(B)** Pericyte nuclei were labelled with DAPI (blue) only, while myoblast nuclei could be identified by the co-labelling of DAPI and GFP (green). Myosin heavy chain (MHC) staining is shown in red. Arrows point towards pericyte nuclei in hybrid MHC$^+$ myotubes in the DAPI channel. Scale bar in overview images = 100 µm. Scale bar in cut-outs = 25 µm. **(C)** Hybrid cultures containing H2B-GFP$^+$ myoblast nuclei and pericyte nuclei were analysed for the presence of MHC$^+$ myotubes to determine the myogenic fusion index (MFI; grey checkered bars). The fraction of pericyte nuclei in MHC$^+$ myotubes is shown in the coloured bars (DM1 pericytes in pink, unaffected pericytes in blue, DM1 myoblasts in dark-green, control myoblasts in light-green). NC is the negative control, where no additional cells were added. There was no significant difference found for MFI between the different hybrid cultures ($p > 0.05$) (three independent differentiation experiments; mean ± SEM; Kruskal-Wallis test) **(D)** Data shown in C, normalized to the MFI of each co-culture. There was no significant difference with regard to disease status ($p > 0.05$), nor cell type ($p > 0.05$) on the normalized contribution (three independent differentiation experiments; mean ± SEM; one-way ANOVA test)

RNA FISH (Fig. 5), MBNL1 (Fig. 6 and DAPI at day 5 of differentiation.

Hybrid cultures generated from DM1 myoblasts and pericytes from unaffected donors (C1 or C2) showed a significant inverse correlation between the average RNA foci count per DM1 H2B-GDP nucleus and the number of pericyte nuclei from unaffected donors in a myotube (Fig. 5A, B; C1: $p = 0.022$, C2: $p < 0.0001$). In contrast, the RNA foci count was not affected by the fraction of pericytes in hybrid myotubes generated from DM1 myoblasts and P4 pericytes ($p > 0.05$). Interestingly, while the number of RNA foci in DM1 derived nuclei decreased with an increasing number of unaffected derived nuclei in the myotube, the mean area of the nuclear foci increased (Fig. 5C; C1: $p < 0.0001$, C2: $p < 0.0001$). No such effect was found for co-cultures with patient derived pericytes (P4: $p > 0.05$). When looking at the total area occupied by foci per DM1 H2B-GFP nucleus in hybrid myotubes, we see significant differences, albeit small and with fluctuating values, and without a clear trend like in Fig. 5C (Suppl. Fig. 1). Notably, no translocation of expanded RNA to unaffected nuclei was ever observed [38].

Next, we quantified MBNL1 protein in both myoblast- and pericyte-originating nuclei in hybrid myotubes, taking the free nuclear MBNL1 staining as a proxy for disease severity. The grey values in nuclear foci were subtracted from the total grey value of nuclear MBNL1, leaving only the value of free MBNL1 per nucleus (Fig. 6A, B). We found that the fusion of unaffected pericytes increased the level of free MBNL1 in DM1 donor nuclei originating from patient myoblasts ($p < 0.0001$). The hybrid culture containing C1 pericytes already showed

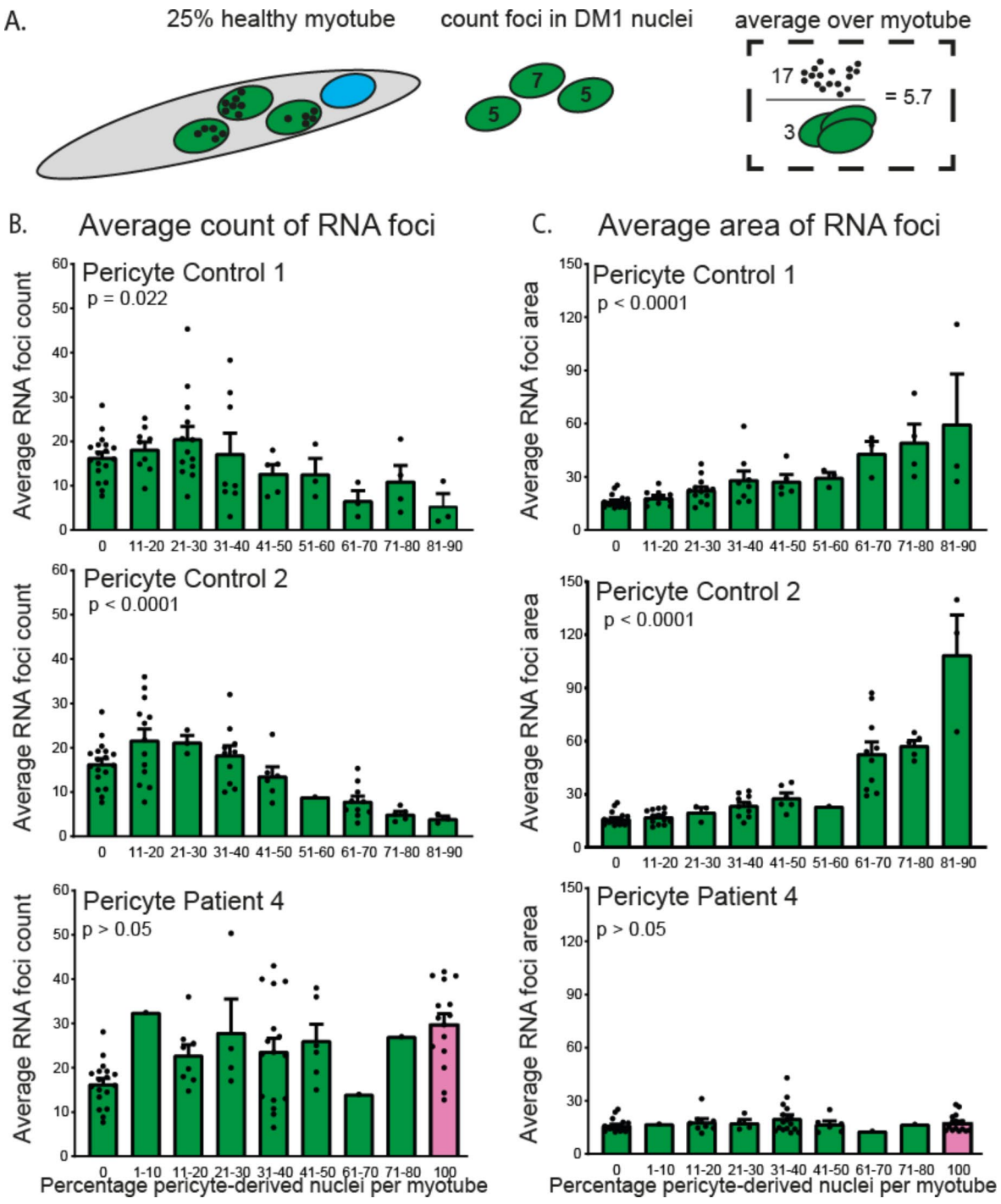

Fig. 5 RNA foci number and size in DM1 nuclei in hybrid myotubes. **(A)** Graphical visualisation of foci count in hybrid cultures based on DM1 myoblasts and either control or patient-derived pericytes. As an example, one myotube containing three DM1 H2B-GFP nuclei (green) and one unaffected primary pericyte nucleus in blue is shown. Foci number was averaged over the DM1 nuclei only. **(B)** Average count of RNA foci in DM1 nuclei per hybrid myotube, using C1 ($p = 0.022$), C2 ($p < 0.0001$) and P4 ($p > 0.05$) pericyte cultures (three independent differentiation experiments; mean ± SEM if applicable; Kruskal-Wallis test). **(C)** Average area of RNA foci in DM1 nuclei per hybrid myotube, based on C1 ($p < 0.0001$), C2 ($p < 0.0001$) and P4 ($p > 0.05$) pericyte cultures (three independent differentiation experiments; mean ± SEM if applicable; Kruskal-Wallis test)

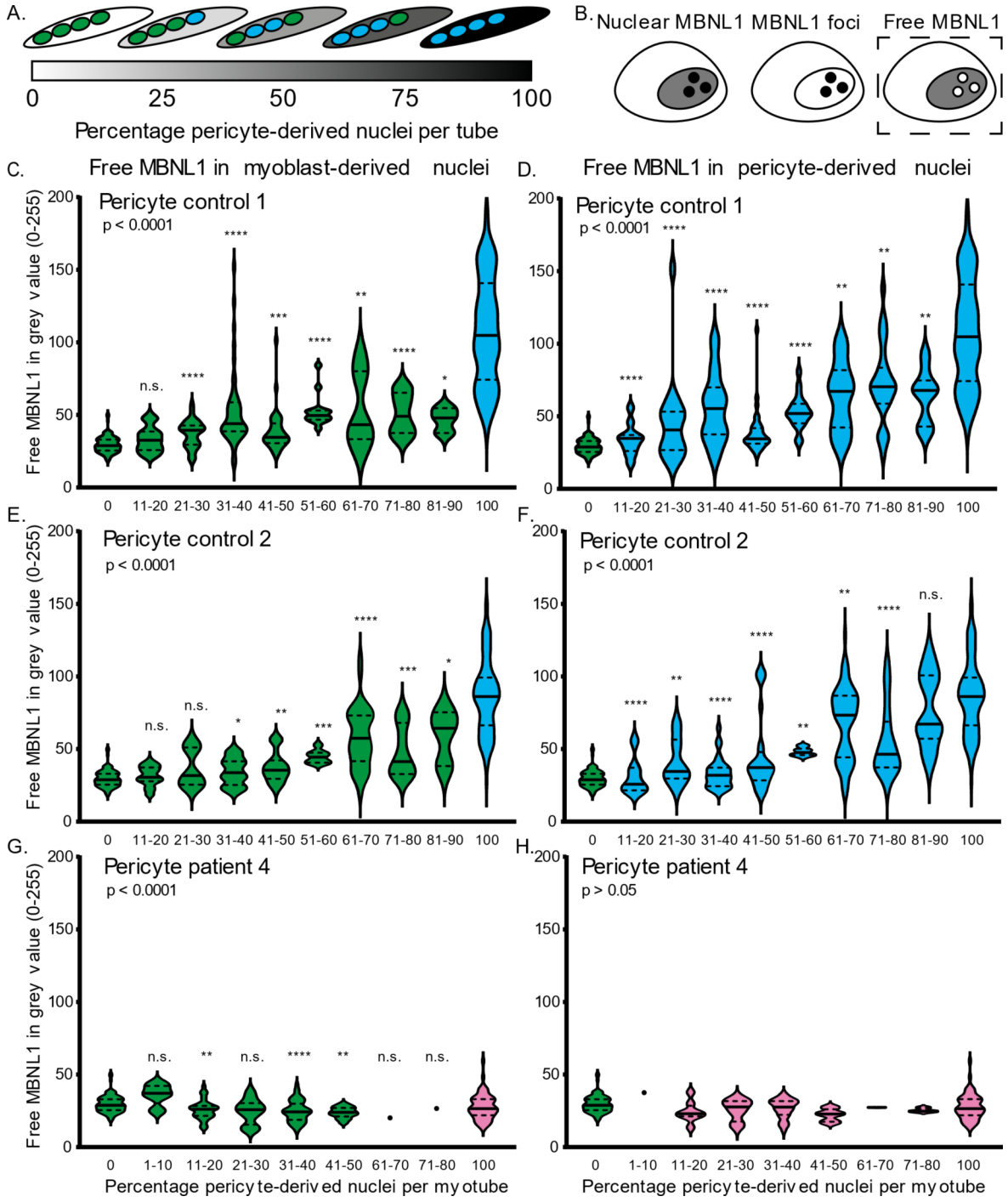

Fig. 6 Free nuclear MBNL1 protein in nuclei in hybrid myotubes. **(A)** A schematic illustration of the range of possible hybrid myotubes in mixed cultures based on DM1 myoblasts and either control or patient-derived pericytes, e.g., from 0–100% nuclei from an unaffected donor, with DM1 H2B-GFP nuclei in green and pericyte nuclei of an unaffected donor in blue. **(B)** Graphic of free MBNL1 calculation. Grey values of total MBNL1 were measured in the nuclei. Next, the grey values of the foci were determined and subtracted from the total grey value, leading to the remaining free MBNL1 abundance in nuclei. **(C-E-G)** Free MBNL1 measured in DM1 nuclei in hybrid myotubes of DM1 myoblasts with pericytes C1 ($p < 0.0001$) **(C)**, C2 ($p < 0.0001$) **(E)**, or P4 ($p < 0.0001$). **(G)**. **(D-F-H)** Free MBNL1 measured in pericyte-derived nuclei in hybrid myotubes of DM1 myoblasts with pericytes C1 ($p < 0.0001$) **(D)**, C2 ($p < 0.0001$) **(F)**, or P4 ($p > 0.05$) **(G)**. All statistical tests were done following a Kruskal-Wallis test, with Dunn's test correction for multiple comparisons when applicable. **(C-E-G)** Shows comparisons to 0% pericytes added, while **(D-F-H)** compares to 100% healthy nuclei

a significant positive effect at >20% pericyte nuclei in a myotube (Fig. 6C), while C2 pericytes showed a positive effect at >30% pericyte nuclei per myotube (Fig. 6E). In contrast, a hybrid culture with DM1 derived pericytes (P4) showed no effect and in some cases a significant reduced effect of free MBNL1 in myoblast-derived DM1 nuclei (Fig. 6G). In turn, in unaffected derived pericyte nuclei (C1 or C2) in hybrid myotubes, we observed the opposite effect. Free MBNL1 levels significantly decreased in unaffected derived pericyte nuclei already if only a few DM1 derived nuclei were present in a hybrid myotube (Fig. 6D, F; C1: >20% DM1 nuclei/myotube; $p<0.01$; C2: >30% DM1 nuclei/myotube; $p<0.0001$). No effect was found on nuclear MBNL1 levels in pericyte nuclei from affected DM1 donor P4 (Fig. 6H; $p>0.05$).

To confirm the spreading of nuclear proteins in myotubes in our system [34], we used co-cultures of DM1 H2B-GFP myoblasts (green) and DMΔ H2B-mCherry myoblasts (red) in which the triplet repeat was removed via gene editing [25]. DMΔ H2B-mCherry myoblasts were added to DM1 H2B-GFP cells at day two of differentiation (comparable to Fig. 4A). The co-cultures were fixed after 5, 10 and 14 days of differentiation and stained for MHC (Fig. 7. While we were still able to determine in the myotubes the origin of each nucleus by its color (green or red) at day 5 and 10, this was impossible after 14 days (Fig. 7) or 20 days (data not shown). Altogether, these observations show that spreading of nuclear proteins between nuclei in hybrid human myotubes exists and that, as a result, disease hallmarks in DM1 myotubes are sensitive to the fusion of myogenic precursor cells from unaffected donors.

Discussion

Previously, we have shown that DM1 patient-derived pericytes maintain normal growth parameters and innate myogenic characteristics in vitro, despite presence of intranuclear $(CUG)_n$ RNA foci [12]. However, it was still unclear if, and when, DM1 disease characteristics would worsen during the path of myogenic differentiation and

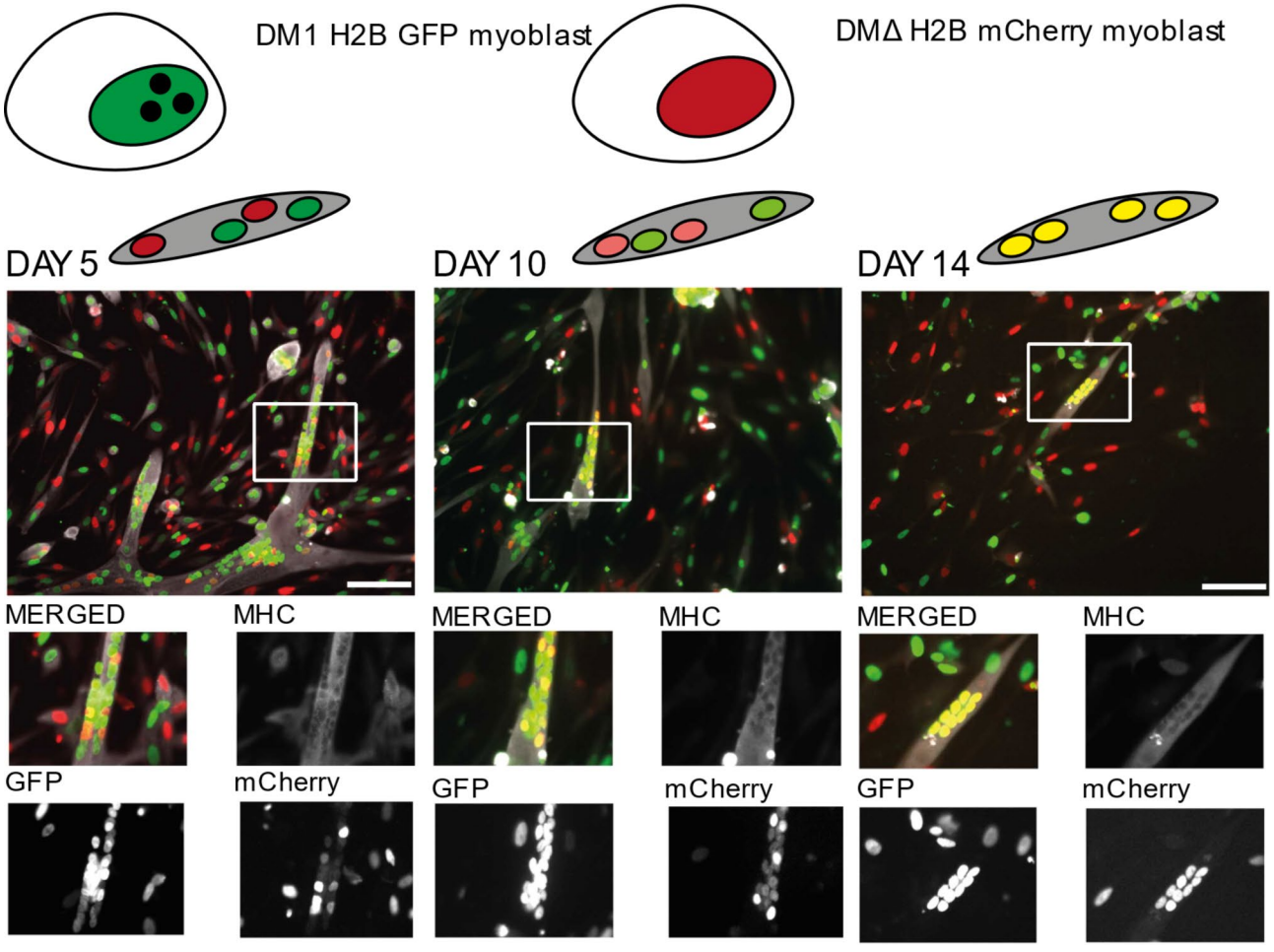

Fig. 7 Spreading of H2B-GFP and H2B-mCherry in hybrid myotubes. Graphical illustration of the experimental set-up, in which DM1 H2B-GFP myoblasts were co-cultured with isogenic DMΔ H2B-mCherry myoblasts. To follow protein spreading over time, differentiating co-cultures were stained 5 to 14 days after addition of the second myoblast line

whether that would affect potential application in cell therapy. Here, we have shown that our pericyte cultures are characterized by various repeat lengths that largely correlate to the number of foci and disease hallmarks. In addition, we have investigated the myogenic potential of these pericytes in a more therapeutically relevant setting. We found that differentiation of pericytes to myotubes was associated with a strongly increased expression of *DMPK*, which led to a robust increase in $(CUG)_n$ RNA- and MBNL1-positive nuclear foci and an overall less diffuse nuclear MBNL1 signal. However, co-cultures of pericytes with H2B-GFP-labelled myoblast-derived myotubes still showed comparable regenerative potential between pericytes carrying DM1 repeat lengths and those carrying non-disease associated repeats. This is in contrast to earlier findings with DM1 myoblasts carrying a repeat associated with congenital DM1, which displayed impaired myogenic fusion capacity [39, 40]. Furthermore, in these co-cultures we show that only a small portion of unaffected nuclei contribute to a major improved effect on RNA foci and MBNL1 protein levels in disease myofibers after only 5 days.

A priori, we did not know which repeat lengths to expect in pericytes, since these cells belong to the microvasculature wrapped around the endothelial cells of postnatal vessels. We determined the $(CTG)_n$ length in pericytes by SP-PCR, which varied between 60 and 950 triplets and also included samples above the detection limit. TP-PCRs performed at diagnosis only provided an estimate of repeat lengths below 200. $(CTG)_n$ repeat length determination by SP-PCR in blood washings of biopsies gave us the ePAL of patients which was closely related to the TP-PCR results and was lower than the modal repeat length in pericytes. It is well known that repeat determination of blood samples generally underestimates repeat length in myogenic cells [2]. Overall, our results show that the repeat lengths in pericytes look more similar to those in myogenic cells than in blood.

While a clear modal repeat length was observed in most pericyte cultures, hybridization signals corresponding to different repeat lengths present at lower levels indicated heterogeneous $(CTG)_n$ expansions within the cell population. These heterogenous $(CTG)_n$ expansions may represent heterogenous expansions in less successful cells of the originating tissue or in vitro variants of cultured progenitors that occurred via replication-independent or replication-dependent pathways such as DNA repair- and transcription related mechanisms [41]. Alternatively, the heterogeneity could have originated from clonal progenitors that have not expanded as rapidly as the primary clones. Primary cell cultures will presumably develop into a select group of clonally expanded cells. Although still a mixed culture, it is possible that in vitro selection occurred of pericytes that expanded well. This clonality must be considered when going forward with a cell therapy approach, as the expansion of primarily a selected group of cells could have important therapeutic implications [16].

DM1 hallmarks were particularly noticeable when pericytes differentiated to myotubes, during which *DMPK* expression increased. Interestingly, P4 cells with 90 and 115 CTG triplets contained on average around 15 foci per nucleus in MHC^+ myotubes, whereas *DMPK* expression did not change much upon differentiation and foci were sparse in mononuclear cells. We assume that this almost sudden appearance of foci relates to the threshold repeat length detection limit in this cell culture and more accessible repeat RNA conformations in ribonucleoprotein complexes in myotube nuclei. Considerable variation was observed in the number of foci between individual pericyte nuclei and pericyte-derived myotube nuclei from one participant, reminiscent of the variation that has been observed previously in myoblast cultures and muscle cell nuclei from biopsies of DM1 patients [39, 42].

In contrast to what was reported earlier in myoblasts, DM1 pericytes did not show a lower intensity MBNL1 signal in the nucleoplasm than cells from unaffected controls [43]. A proxy for disease severity at the cellular level, nucleoplasmic MBNL1 signal decreased only upon the formation of myotubes during differentiation. This observation suggests that *DMPK* expression in proliferative pericytes is not high enough to affect the free nuclear MBNL1 protein distribution, or that other downstream factors or mechanisms preclude initiation of DM1 disease mechanisms at this cell stage.

Pericytes are known to contribute to muscle regeneration [44]. We validated this process in co-culture experiments including pericytes and GFP-labelled myoblasts. All observations were based on single cell or single nucleus observations. Technical limitations inherent to the use of differentiated (co-)cultures, namely, differentiation rate, mixed cell types, and composition of hybrid myotubes, limited the amount of disease hallmarks that could be studied. Despite the presence of DM1 disease biomarkers, all patient-derived pericytes maintained comparable myogenic regeneration potential to myoblasts. Thereby underscoring the suitability of pericytes for therapeutic applications. Using hybrid cultures of unaffected pericytes and patient-derived GFP-labelled myoblasts, DM1 disease hallmarks were significantly downregulated by the addition of unaffected nuclei to DM1 myotubes. The average count of RNA foci in DM1 nuclei decreased, while the amount of free MBNL1 increased, as more nuclei from unaffected pericytes participated in myotube formation.

Although the foci number in DM1 nuclei was reduced upon fusion with unaffected pericytes, their estimated size more than doubled. Our hypothesis is that the

growth of RNA foci is due to the influx of additional MBNL1 protein from the sarcoplasm, leading to a change in the intranuclear concentration of macromolecules. RNA foci may thus become oversaturated and a biomolecular condensate of RNA and MBNL1 aggregated protein may be formed via phase separation [45]. Unfolding of the expanded RNA may in addition lead to a larger surface being able to be reached by the $(CAG)_6$ probe. Despite the fact that we provide evidence for the spreading of proteins encoded by a certain nucleus to other nuclei in the same myotube due to the shared cytoplasm, we never observed RNA foci in unaffected nuclei in hybrid myotubes, and thus have no evidence for internuclear transport of expanded RNA in our cell model [38].

In summary, we demonstrate here how pericytes with various repeat expansions behave in proliferative, differentiated and regenerative states. Unaffected pericytes are able to downregulate disease markers in DM1 myotube nuclei after only five days of culture. This means that there is a possibility to neutralize the negative effects of MBNL1 sequestration in existing myofibers in patients, stipulating the potential of cell therapy for DM1. In an ideal situation in vivo, pericytes will not only fuse with diseased, regenerating muscle and upregulate free MBNL1, but also take the niche position of satellite cells in muscle tissue. In doing so, the stem cell population can be corrected and provides numerous unaffected myogenic progenitors that support sustainable regeneration of skeletal muscles affected in patients. Before this scenario becomes reality, more research is required to examine the long-term survival and myogenic potential of transplanted pericytes in an in vivo setting.

Supplementary Information

The online version contains supplementary material available at https://doi.org/10.1186/s13287-024-03913-y.

Supplementary Material 1

Acknowledgements

We sincerely thank Denis Furling and Vincent Mouly for supplying the DM1 immortalized human myoblasts. We also thank Fran Smulders, Yvonne Cornelissen, and Tim Schreuder for retrieving biopsies from the eight individuals from whom pericytes have been isolated. We thank the other members of the myotonic dystrophy group for input and support. ChatGPT was occasionally utilized to verify the correctness and proper usage of the English language.

Authors' contributions

Conceptualization, R.H.L.R., C.R.M.A., M.W., B.G.M.v.E., H.v.B., and D.G.W.; Investigation, R.H.L.R., C.R.M.A., M.W. and S.A.C.; Formal Analysis, R.H.L.R., C.R.M.A., M.W., S.A.C., D.G.M., H.v.B., and D.G.W.; Writing – Original Draft, R.H.L.R, C.R.M.A, H.v.B., and D.G.W.; Writing – Review and Editing, R.H.L.R, C.R.M.A, M.W., S.A.C., D.G.M., H.v.B., and D.G.W.; Visualization, R.H.L.R, C.R.M.A, M.W., S.A.C., D.G.M., H.v.B., and D.G.W.; Supervision, H.v.B. and D.G.W. All authors read and approved the final manuscript.

Funding

This work was funded by the Donders Institute for Brain Cognition and Behaviour, Radboud university medical center and Prinses Beatrix Spierfonds (grant numbers W.OR18-18 and W.OR20-03; with contribution from Stichting Spieren voor Spieren).

Data availability

After acceptance of the manuscript for publication, datasets supporting the conclusions of this article will be made available in the Radboud Data Repository upon reasonable request.

Declarations

Ethics approval and consent to participate

As described earlier, the human biopsy procedure including the cell culture protocol was approved by the local committee on Research Involving Human Subjects (METC Oost-Nederland; Commissie Mensgebonden Onderzoek (CMO) 2016–2451, NL57509.091.16), entitled "Development of an autologous myogenic cell therapy against the neuromuscular phenotype of myotonic dystrophy type 1", approval date 18th of October 2016 [12]. Informed consent to participate in our study was obtained from all participants. No adverse events following the biopsy procedure were reported.

Consent for publication

All authors confirm their consent for publication.

Competing interests

Several authors of this publication are members of the Radboudumc Center of Expertise for neuromuscular disorders (Radboud-NMD), Netherlands Neuromuscular Center (NL-NMD) and the European Reference Network for rare neuromuscular diseases (EURO-NMD). Within the last 36 months, D.G.W. has been a scientific consultant and/or received an honoraria/grants from Design Therapeutics and Synaffix. Within the last 36 months D.G.M. has been a scientific consultant and/or received an honoraria/grants from AMO Pharma, Dyne, F. Hoffman-La Roche, LoQus23, MOMA Therapeutics, Novartis, Ono Pharmaceuticals, Pfizer Pharmaceuticals, Rgenta Therapeutics, Sanofi, Sarepta Therapeutics Inc, Script Biosciences, Triplet Therapeutics, and Vertex Pharmaceuticals. D.G.M. also had/has research contracts with AMO Pharma and Vertex Pharmaceuticals. B.G.M.v.E. reports grants from or contracts with Prinses Beatrix Spierfonds, the Dutch FSHD Foundation, and Stichting Spieren voor Spieren, royalties and licenses from patent EP2012740236, and institutional payments for consulting and participation on data safety monitoring and advisory boards from Fulcrum Therapeutics, Facio, Avidity, Dyne, Arrowhead, Biomarin, Pepgen, and Teva.

Author details

[1]Donders Institute for Brain Cognition and Behaviour, Department of Human Genetics, Radboud university medical center, Nijmegen 6500 HB, The Netherlands
[2]Donders Institute for Brain Cognition and Behaviour, Department of Neurology, Radboud university medical center, Nijmegen 6500 HB, The Netherlands
[3]Department of Medical BioSciences, Radboud university medical center, Radboud Institute for Medical Innovation, Nijmegen 6500 HB, The Netherlands
[4]School of Molecular Biosciences, College of Medical, Veterinary and Life Sciences, University of Glasgow, Glasgow, UK

Received: 5 July 2024 / Accepted: 1 September 2024
Published online: 15 September 2024

References

1. De Antonio M, Dogan C, Hamroun D, Mati M, Zerrouki S, Eymard B, et al. Unravelling the myotonic dystrophy type 1 clinical spectrum: a systematic registry-based study with implications for disease classification. Rev Neurol-France. 2016;172(10):572–80.
2. Thornton CA, Johnson K, Moxley RT. 3rd. Myotonic dystrophy patients have larger CTG expansions in skeletal muscle than in leukocytes. Ann Neurol. 1994;35(1):104–7.

3. Joseph JT, Richards CS, Anthony DC, Upton M, Perez-Atayde AR, Greenstein P. Congenital myotonic dystrophy pathology and somatic mosaicism. Neurology. 1997;49(5):1457–60.
4. Cumming SA, Jimenez-Moreno C, Okkersen K, Wenninger S, Daidj F, Hogarth F, et al. Genetic determinants of disease severity in the myotonic dystrophy type 1 OPTIMISTIC cohort. Neurology. 2019;93(10):e995–1009.
5. de Pontual L, Tomé S. Overview of the Complex relationship between Epigenetics Markers, CTG repeat instability and symptoms in myotonic dystrophy type 1. Int J Mol Sci. 2022;23(7).
6. Teplova M, Patel DJ. Structural insights into RNA recognition by the alternative-splicing regulator muscleblind-like MBNL1. Nat Struct Mol Biol. 2008;15(12):1343–51.
7. Sznajder LJ, Swanson MS. Short Tandem repeat expansions and RNA-Mediated pathogenesis in myotonic dystrophy. Int J Mol Sci. 2019;20(13).
8. Pascual-Gilabert M, Artero R, Lopez-Castel A. The myotonic dystrophy type 1 drug development pipeline: 2022 edition. Drug Discov Today. 2023;28(3):103489.
9. De Serres-Bérard T, Benichou SA, Jauvin D, Boutjdir M, Puymirat J, Chahine M. Recent Progress and challenges in the development of antisense therapies for myotonic dystrophy type 1. Int J Mol Sci. 2022;23(21).
10. Pierantozzi E, Vezzani B, Badin M, Curina C, Severi FM, Petraglia F, et al. Tissue-specific cultured human pericytes: Perivascular Cells from smooth muscle tissue have restricted mesodermal differentiation ability. Stem Cells Dev. 2016;25(9):674–86.
11. Quattrocelli M, Palazzolo G, Floris G, Schoffski P, Anastasia L, Orlacchio A, et al. Intrinsic cell memory reinforces myogenic commitment of pericyte-derived iPSCs. J Pathol. 2011;223(5):593–603.
12. Ausems CRM, Raaijmakers RHL, van den Broek W, Willemse M, van Engelen BGM, Wansink DG, van Bokhoven H. Intrinsic myogenic potential of skeletal muscle-derived pericytes from patients with myotonic dystrophy type 1. Mol Ther Methods Clin Dev. 2019;15:120–32.
13. Chen CW, Montelatici E, Crisan M, Corselli M, Huard J, Lazzari L, Peault B. Perivascular multi-lineage progenitor cells in human organs: regenerative units, cytokine sources or both? Cytokine Growth Factor Rev. 2009;20(5–6):429–34.
14. Tedesco FS, Dellavalle A, Diaz-Manera J, Messina G, Cossu G. Repairing skeletal muscle: regenerative potential of skeletal muscle stem cells. J Clin Invest. 2010;120(1):11–9.
15. King NE, Courtney JM, Brown LS, Fortune AJ, Blackburn NB, Fletcher JL, et al. Induced pluripotent stem cell derived pericytes respond to mediators of proliferation and contractility. Stem Cell Res Ther. 2024;15(1):59.
16. Ausems CRM, van Engelen BGM, van Bokhoven H, Wansink DG. Systemic cell therapy for muscular dystrophies: the ultimate transplantable muscle progenitor cell and current challenges for clinical efficacy. Stem Cell Rev Rep. 2021;17(3):878–99.
17. Cossu G, Previtali SC, Napolitano S, Cicalese MP, Tedesco FS, Nicastro F, et al. Intra-arterial transplantation of HLA-matched donor mesoangioblasts in Duchenne muscular dystrophy. EMBO Mol Med. 2015;7(12):1513–28.
18. Gerli MF, Maffioletti SM, Millet Q, Tedesco FS. Transplantation of induced pluripotent stem cell-derived mesoangioblast-like myogenic progenitors in mouse models of muscle regeneration. J Vis Exp. 2014;83:e50532.
19. Sampaolesi M, Blot S, D'Antona G, Granger N, Tonlorenzi R, Innocenzi A, et al. Mesoangioblast stem cells ameliorate muscle function in dystrophic dogs. Nature. 2006;444(7119):574–9.
20. Sampaolesi M, Torrente Y, Innocenzi A, Tonlorenzi R, D'Antona G, Pellegrino MA, et al. Cell therapy of alpha-sarcoglycan null dystrophic mice through intra-arterial delivery of mesoangioblasts. Science. 2003;301(5632):487–92.
21. Galvez BG, Sampaolesi M, Brunelli S, Covarello D, Gavina M, Rossi B, et al. Complete repair of dystrophic skeletal muscle by mesoangioblasts with enhanced migration ability. J Cell Biol. 2006;174(2):231–43.
22. van Tienen F, Zelissen R, Timmer E, van Gisbergen M, Lindsey P, Quattrocelli M, et al. Healthy, mtDNA-mutation free mesoangioblasts from mtDNA patients qualify for autologous therapy. Stem Cell Res Ther. 2019;10(1):405.
23. Gudde AE, Gonzalez-Barriga A, van den Broek WJ, Wieringa B, Wansink DG. A low absolute number of expanded transcripts is involved in myotonic dystrophy type 1 manifestation in muscle. Hum Mol Genet. 2016;25(8):1648–62.
24. Zelissen R, Ahmadian S, Montilla-Rojo J, Timmer E, Ummelen M, Hopman A et al. Fusion of Wild-Type mesoangioblasts with myotubes of mtDNA Mutation Carriers leads to a proportional reduction in mtDNA mutation load. Int J Mol Sci. 2023;24(3).
25. van Agtmaal EL, Andre LM, Willemse M, Cumming SA, van Kessel IDG, van den Broek W, et al. CRISPR/Cas9-Induced (CTGCAG)n repeat instability in the myotonic dystrophy type 1 locus: implications for therapeutic genome editing. Mol Ther. 2017;25(1):24–43.
26. Zhu CH, Mouly V, Cooper RN, Mamchaoui K, Bigot A, Shay JW, et al. Cellular senescence in human myoblasts is overcome by human telomerase reverse transcriptase and cyclin-dependent kinase 4: consequences in aging muscle and therapeutic strategies for muscular dystrophies. Aging Cell. 2007;6(4):515–23.
27. Ilina O, Gritsenko PG, Syga S, Lippoldt J, La Porta CAM, Chepizhko O, et al. Cell-cell adhesion and 3D matrix confinement determine jamming transitions in breast cancer invasion. Nat Cell Biol. 2020;22(9):1103–15.
28. Slaats J, Wagena E, Smits D, Berends AA, Peters E, Bakker GJ, et al. Adenosine A2a receptor antagonism restores additive cytotoxicity by cytotoxic T cells in metabolically perturbed tumors. Cancer Immunol Res. 2022;10(12):1462–74.
29. Gomes-Pereira M, Bidichandani SI, Monckton DG. Analysis of unstable triplet repeats using small-pool polymerase chain reaction. Methods Mol Biol. 2004;277:61–76.
30. Monckton DG, Wong LJ, Ashizawa T, Caskey CT. Somatic mosaicism, germline expansions, germline reversions and intergenerational reductions in myotonic dystrophy males: small pool PCR analyses. Hum Mol Genet. 1995;4(1):1–8.
31. Cumming SA, Hamilton MJ, Robb Y, Gregory H, McWilliam C, Cooper A, et al. De novo repeat interruptions are associated with reduced somatic instability and mild or absent clinical features in myotonic dystrophy type 1. Eur J Hum Genet. 2018;26(11):1635–47.
32. Holt I, Mittal S, Furling D, Butler-Browne GS, Brook JD, Morris GE. Defective mRNA in myotonic dystrophy accumulates at the periphery of nuclear splicing speckles. Genes Cells. 2007;12(9):1035–48.
33. Schmidt U, Weigert M, Broaddus C, Myers G, editors. Cell detection with Star-Convex polygons. Cham: Springer International Publishing; 2018.
34. Ferreboeuf M, Mariot V, Furling D, Butler-Browne G, Mouly V, Dumonceaux J. Nuclear protein spreading: implication for pathophysiology of neuromuscular diseases. Hum Mol Genet. 2014;23(15):4125–33.
35. Ballester-Lopez A, Linares-Pardo I, Koehorst E, Nunez-Manchon J, Pintos-Morell G, Coll-Canti J et al. The Need for Establishing a Universal CTG Sizing Method in Myotonic Dystrophy Type 1. Genes-Basel. 2020;11(7).
36. Braida C, Stefanatos RK, Adam B, Mahajan N, Smeets HJ, Niel F, et al. Variant CCG and GGC repeats within the CTG expansion dramatically modify mutational dynamics and likely contribute toward unusual symptoms in some myotonic dystrophy type 1 patients. Hum Mol Genet. 2010;19(8):1399–412.
37. Ausems CRM. First steps towards a pericyte-based muscle therapy for myotonic dystrophy. Nijmegen, The Netherlands: Radboud university; 2022.
38. Mondragon-Gonzalez R, Azzag K, Selvaraj S, Yamamoto A, Perlingeiro RCR. Transplantation studies reveal internuclear transfer of toxic RNA in engrafted muscles of myotonic dystrophy 1 mice. EBioMedicine. 2019;47:553–62.
39. Andre LM, van Cruchten RTP, Willemse M, Bezstarosti K, Demmers JAA, van Agtmaal EL et al. Recovery in the myogenic program of congenital myotonic dystrophy myoblasts after excision of the expanded (CTG)n repeat. Int J Mol Sci. 2019;20(22).
40. Arandel L, Polay Espinoza M, Matloka M, Bazinet A, De Dea Diniz D, Naouar N, et al. Immortalized human myotonic dystrophy muscle cell lines to assess therapeutic compounds. Dis Model Mech. 2017;10(4):487–97.
41. Depienne C, Mandel JL. 30 years of repeat expansion disorders: what have we learned and what are the remaining challenges? Am J Hum Genet. 2021;108(5):764–85.
42. Michel L, Huguet-Lachon A, Gourdon G. Sense and antisense DMPK RNA foci accumulate in DM1 tissues during development. PLoS ONE. 2015;10(9):e0137620.
43. Andre LM, van Cruchten RTP, Willemse M, Wansink DG. (CTG)n repeat-mediated dysregulation of MBNL1 and MBNL2 expression during myogenesis in DM1 occurs already at the myoblast stage. PLoS ONE. 2019;14(5):e0217317.
44. Dellavalle A, Sampaolesi M, Tonlorenzi R, Tagliafico E, Sacchetti B, Perani L, et al. Pericytes of human skeletal muscle are myogenic precursors distinct from satellite cells. Nat Cell Biol. 2007;9(3):255–67.
45. Gao Y, Li X, Li P, Lin Y. A brief guideline for studies of phase-separated biomolecular condensates. Nat Chem Biol. 2022;18(12):1307–18.

Publisher's note